JNS 2 (2012) 61-68

Journal of
NANOSTRUCTURES

JNS
NANOSTRUCTURES
JNS.kashanu.ac.ir

Laminar Mixed Convection of Al_2O_3-Water Nanofluid in a Three-Dimensional Microchannel

G. A. Sheikhzadeh*, M. Ebrahim Qomi, N. Hajialigol*, A. Fattahi

Department of Mechanical Engineering, University of Kashan,Ghotb Ravandi Blvd, Kashan, 87317-51167, Iran.

Article history:
Received 27/3/2012
Accepted 26/5/2012
Published online 1/6/2012

Keywords:
Mixed convection
Microchannel
Nanofluid
Microchannel
Alumina

**Corresponding author:*
E-mail address:
Najmeh.Hajialigol@Gmail.com

Abstract

The fluid flow and heat transfer in a three-dimensional microchannel filled with Al_2O_3- water nanofluid is numerically investigated. The hybrid scheme is used to discretize the convection terms and SIMPLER algorithm is adopted to couple the velocity and pressure field in the momentum equations. The temperature fields, variation of horizontal velocity along the centre line of the channel, average Nusselt number and the thermal resistance in different aspect ratios are presented. It is observed that aspect ratio mainly affected the temperature gradient as well as heat transfer. Analyzing the results of numerical simulations indicates that with increasing aspect ratio, horizontal velocity along the centre line increased and then, average Nusselt number and the inlet and outlet thermal resistance decrease in the microchannel.

1. Introduction

Over two decades ago, microchannels emerged as a potential solution for dissipating thermal energy from densely packed integrated circuitry. Researches indicated that high heat fluxes could be dissipated by a working fluid passing through microchannels that offer an increased surface area to volume ratio. In the early 1980s, Tuckerman and Pease [1] reported that a microchannel heat sink could dissipate as much as 790 W/cm^2 with 71 K mean fluid temperature rise. Because of high heat flux produced by compact integrated circuitries, there is a growing necessity for novel researches into design, performance, and application of microchannel.

Li and Peterson [2] proposed a three-dimensional semi-normalized numerical method to explore the optimal geometry of the parallel microchannel heat sinks and demonstrated that on a silicon wafer with a typical thickness of 450 μm, the configurations first used by Tuckerman and Pease [1] and by Kawano et al. [3], were quite

close to the optimized values predicted by the numerical model. Nevertheless, the ultimate optimal geometry was not achieved due to the constraint of the wafer thickness of 450 µm. Tullius et al. [4] comprehensively reviewed the cooling performance of microchannels with various designs and different fluids. Air, water and fluoro-chemicals are the most common fluids used in their microchannels. The heat transfer performance of these fluids is limited, however, due to their transport properties and/or low thermal conductivity.

To enhance the thermal conductivity of working liquids and accordingly further improving in performance of the liquid-cooled microchannel heat sinks, the application of nanofluids in microchannels has gained much attention in recent years. Lee and Choi [5] have found that the nanofluid in the microchannel heat exchanger dramatically enhances cooling rate compared with the conventional water cooled and liquid-nitrogen-cooled microchannel heat exchangers. In a numerical hydrodynamic and thermal study of laminar fully developed flows of copper– and diamond–water nanofluids [6], the cooling performance of the microchannel heat sink was found significantly improved as reflected by the marked reduction in the thermal resistance as well as the temperature difference between the heated microchannel wall and the nanofluids. Raisi et al. [7] numerically studied the forced convection of a laminar nanofluid in a microchannel in both slip and no-slip conditions. They argued that making use of nanofluids enhances the heat transfer performance of the microchannel. Aminossadati et al. [8] studied effects of magnetic field on nanofluid forced convection in a partially heated microchannel. Their results showed that the microchannel heat is more transferred at higher values of the Reynolds numbers and magnetic field.

The main objective of this work is to investigate the heat transfer performance of a water– Al_2O_3 nanofluid in the three- dimensional microchannel in various microchannel aspect ratios. The hybrid scheme is used to discretize the convection terms and SIMPLER algorithm is adopted to couple the velocity and pressure field in the momentum equations.

2. Geometry and Boundary Conditions

Fig. 1 shows a schematic diagram of the three-dimensional microchannel considered in this study according to work of Mlcak et al. [9]. It is assumed that the microchannel is manufactured by Silicon. Dimensions of the schematic geometry are shown in Tables 1 and 2. Microchannel surface aspect ratios (Ar) are w_c/h_c = 0.1, 0.5 and 1 and hydraulic diameter (D_h) of that is 86.6 µm. The bottom surface with dimensions of w×l is heated with a constant and uniform heat flux of q´´= 90 kw/m^2. The other michrochannel walls are thermally insulated. The temperature of the water–Al_2O_3 nanofluid at the microchannel inlet is T_c = 298 K.

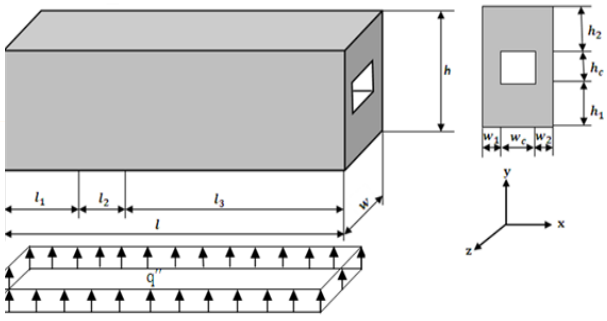

Fig. 1. A schematic geometry of the physical model.

Table 1. Dimensions of the microchannel (μm).

h	l	l_1	l_2	w
900	10000	3478	4348	100

Table 2. Dimensions of the microchannel surface in various Ar (μm).

$Ar=w_c/h_c$	h_c	w_c
0.1	476	47.6
0.5	130	64.9
1	86.6	86.6

3. Governing Equations and Numerical Procedure

The non-dimensional governing equations of continuity, momentum and energy equations are presented as follows:

Continuity equation:

$$\frac{\partial U}{\partial X}+\frac{\partial V}{\partial Y}+\frac{\partial W}{\partial Z}=0 \quad (1)$$

X-momentum equation:

$$U\frac{\partial U}{\partial X}+V\frac{\partial U}{\partial Y}+W\frac{\partial U}{\partial Z}=-\frac{\partial P}{\partial X}+\frac{1}{Re\times\vartheta_f\times\rho_{nf,0}}\left[\frac{\partial}{\partial X}\left(\mu_{nf}\frac{\partial U}{\partial X}\right)+\frac{\partial}{\partial Y}\left(\mu_{nf}\frac{\partial U}{\partial Y}\right)+\frac{\partial}{\partial Z}\left(\mu_{nf}\frac{\partial U}{\partial Z}\right)\right] \quad (2)$$

Y-momentum equation:

$$U\frac{\partial V}{\partial X}+V\frac{\partial V}{\partial Y}+W\frac{\partial V}{\partial Z}=-\frac{\partial P}{\partial Y}+\frac{1}{Re\times\vartheta_f\times\rho_{nf,0}}\left[\frac{\partial}{\partial X}\left(\mu_{nf}\frac{\partial V}{\partial X}\right)+\frac{\partial}{\partial Y}\left(\mu_{nf}\frac{\partial V}{\partial Y}\right)+\frac{\partial}{\partial Z}\left(\mu_{nf}\frac{\partial V}{\partial Z}\right)\right]+\frac{(\rho\beta)_{nf}}{\beta_f\rho_{nf,o}}Ri\theta \quad (3)$$

Z-momentum equation:

$$U\frac{\partial W}{\partial X}+V\frac{\partial W}{\partial Y}+W\frac{\partial W}{\partial Z}=-\frac{\partial P}{\partial Z}+\frac{1}{Re\times\vartheta_f\times\rho_{nf,0}}\left[\frac{\partial}{\partial X}\left(\mu_{nf}\frac{\partial W}{\partial X}\right)+\frac{\partial}{\partial Y}\left(\mu_{nf}\frac{\partial W}{\partial Y}\right)+\frac{\partial}{\partial Z}\left(\mu_{nf}\frac{\partial W}{\partial Z}\right)\right] \quad (4)$$

Energy equations:

$$U\frac{\partial\theta}{\partial X}+V\frac{\partial\theta}{\partial Y}+W\frac{\partial\theta}{\partial Z}=\frac{1}{Re\times Pr\times\alpha_f\times(\rho c_p)_{nf}}\left[\frac{\partial}{\partial X}\left(K_{nf}\frac{\partial\theta}{\partial X}\right)+\frac{\partial}{\partial Y}\left(K_{nf}\frac{\partial\theta}{\partial Y}\right)+\frac{\partial}{\partial Z}\left(K_{nf}\frac{\partial\theta}{\partial Z}\right)\right] \quad (5)$$

$$\left[\frac{\partial}{\partial X}\left(K_s\frac{\partial\theta}{\partial X}\right)+\frac{\partial}{\partial Y}\left(K_s\frac{\partial\theta}{\partial Y}\right)+\frac{\partial}{\partial Z}\left(K_s\frac{\partial\theta}{\partial Z}\right)\right]=0 \quad (6)$$

In the above equations, the following non-dimensional parameters are used:

$$X=\frac{x}{D_h} \qquad Y=\frac{y}{D_h}$$
$$Z=\frac{z}{D_h} \qquad U=\frac{u}{u_c}$$
$$V=\frac{v}{u_c} \qquad W=\frac{w}{u_c} \quad (7)$$
$$P=\frac{p}{\rho_{nf}u_c^2} \qquad \theta=\frac{T-T_C}{\Delta T}$$

where, U, V and W are the velocity components, P the pressure, θ the temperature, ρ the density, g the gravitational acceleration, ν the dynamic viscosity and β the coefficient of thermal expansion. The properties of the nanofluid can be defined based on the properties of water and Alumina:

$$\rho_{nf}=(1-\varphi)\rho_f+\varphi\rho_{np} \quad (8)$$

$$(\rho c_p)_{nf}=(1-\phi)(\rho c_p)_f+\phi(\rho c_p)_{np} \quad (9)$$

$$\alpha_{nf}=\frac{k_{nf}}{(\rho c_p)_{nf}} \quad (10)$$

Here, φ is the volume fraction of nanoparticles, and the subscripts f, nf and np stand for base fluid, nanofluid and nanoparticles, respectively. The effective thermal conductivity of the nanofluid calculated by the Chon et al. model [10] is:

$$\frac{k_{nf}}{k_f}=1+64.7\varphi^{0.4076}\left(\frac{d_f}{d_p}\right)^{0.3690}\left(\frac{k_p}{k_f}\right)^{0.7476}Pr_T^{0.9955}Re^{1.2321} \quad (11)$$

Here Pr_T and Re are defined by:

$$Pr_T=\frac{\mu_f}{\rho_f\alpha_f} \quad (12)$$

$$Re=\frac{\rho_f k_b T}{3\pi\mu_f l_f} \quad (13)$$

k_b=1.3807×10-23 J/K, is the Boltzmann constant and l_f =0.17 nm is the mean path of fluid particles [10]. The viscosity of the nanoparticle (Al_2O_3) as given by Nguyen et al. [10] is:

$$\mu_{nf}=\exp(3.003-0.04203T-0.5445\varphi+.00002553T^2+0.0524\varphi^2-1.622\varphi^{-1})\times10^{-3} \quad (14)$$

The temperature in Eq. (14) is expressed by Celsius. Nusselt number on the bottom surface is calculated as follows:

$$Nu_s = \frac{\frac{\Delta T k_f}{D_h} D_h}{k_f(\theta_{w,m}(X) \times \Delta T - \theta_m(X) \times \Delta T)} = \frac{1}{(\theta_{w,m}(X) - \theta_m(X))} \quad (15)$$

where:

$$\theta_{w,m}(X) \times \Delta T = \frac{\Delta T}{p_s} \int \theta_w(Y,Z) dS \quad (16)$$

$$\theta_m(X) \times \Delta T = \frac{\Delta T}{U_m A_c} \int_{L_1}^{L_2} \int_{H_1}^{H_2} U(Y,Z)\theta(Y,Z) dY dZ \quad (17)$$

$$U_m = \frac{\int_{L_1}^{L_2} \int_{H_1}^{H_2} U(X,Y) dY dZ}{\int_{L_1}^{L_2} \int_{H_1}^{H_2} dY dZ} \quad (18)$$

Here, P_s and S are channel perimeter and surface along channel perimeter, respectively. The subscript w stands for microchannel wall. Finally, the average Nusselt number on the bottom surface is determined from:

$$Nu_{avg} = \frac{\int_0^l \frac{dX}{(\theta_{w,m}(X) - \theta_m(X))}}{\int_0^l dX} \quad (19)$$

The inlet and outlet thermal resistance value, R, as defined by Eqs (20) and (21) was used to monitor the behavior of the temperature field.

$$R_{inlet} = \frac{\theta_{wmax,inlet} \Delta T}{\frac{\Delta T k_f}{D_h}} = \frac{D_h \theta_{wmax,inlet}}{k_f} \quad (20)$$

$$R_{outlet} = \frac{\theta_{wmax,outlet} \Delta T}{\frac{\Delta T k_f}{D_h}} = \frac{D_h \theta_{wmax,outlet}}{k_f} \quad (21)$$

The governing equations associated with the boundary conditions are numerically solved using the control-volume based on finite volume method. The hybrid-scheme, which is a combination of the central difference scheme and the upwind scheme, is used to discretize the convection terms. In order to couple the velocity and pressure field in the momentum equations, the well- known SIMPLER-algorithm was adopted. Grid independency of the solution is investigated for the standard case. The solution of the fully coupled discretized equations is obtained iteratively using TDMA method. In this study, various grid sizes are tested to guarantee a grid independent solution for Ar = 0.1. It is found that a grid size of 141×71×31 ensures a grid independent solution.

4. Results and Discussion

The accuracy of results is verified by comparison the results with the available data published by Aminossadati et al. [8] as depicted in Figs. 2 and 3. In these figures, red and black lines are for the present and reference results, respectively. In addition, Table 2 compares the average Nusselt number obtained by the present study with those of Lo et al. [11] in a three- dimensional cavity. The current results are in good agreement with references results.

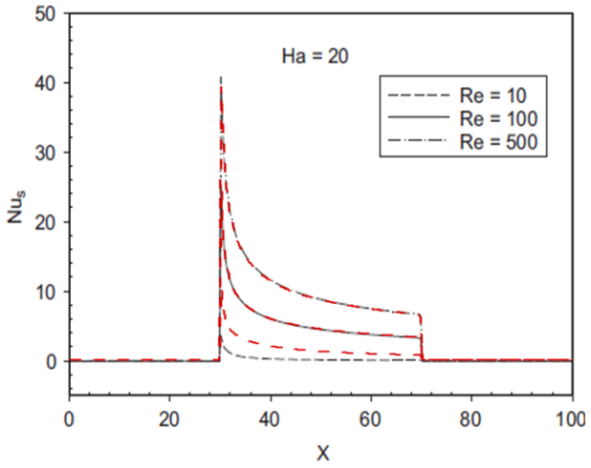

Fig. 2. Variation of local Nusselt number along the channel length (red and black lines are for the present work and reference results).

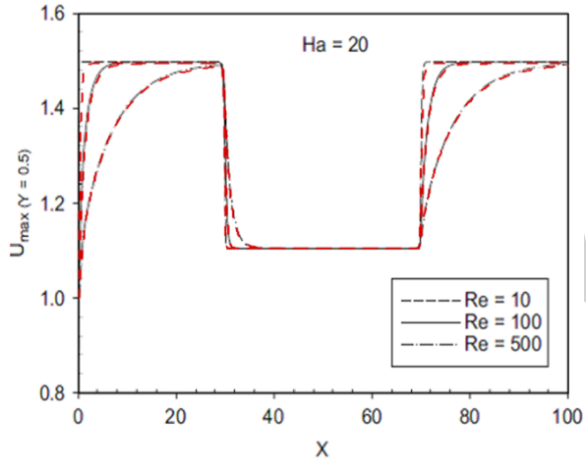

Fig. 3. Variation of horizontal velocity along the centreline of the channel (red and black lines are for the present work and reference results).

Table 3. Average Nusselt number: comparison between the present work and data of Lo et al. [9].

Ra	10^3	10^4	10^5
Present work	1.0715	2.0623	4.03853
Lo et al. [9]	1.0884	2.0537	4.03329

The numerical analysis is carried out to find the influence of aspect ratio on mixed convection in the three- dimensional microchannel. The study is done for $0.1 \leq Ar \leq 1$, $50 \leq Re \leq 400$, $\varphi=0.02$ and Pr = 6.2. The temperature fields, variation of horizontal velocity along the centreline of the channel, average Nusselt number and the thermal resistance are presented. Temperature distributions for various aspect ratios and Re=200 in X=30, 55, 70 and 100 are illustrated in Fig. 4. This figure shows that for all values of Ar, the temperature in both the nanofluid and the microchannel wall solid rise with increasing distance from the channel entrance. It is also evident that the high temperature regions in the walls of the microchannel increase as Ar increases. The horizontal lines observed in the microchannel wall are demonstrator of conduction heat transfer.

Fig. 5 shows the variation of the maximum dimensionless horizontal velocity (U_{max}) versus the channel centre line for three values of Ar and Re=200. As revealed in Fig. 5, U_{max} increases as Ar rises. This can be explained by increasing recirculation area (or cross section of microchannel) that increases the amount of flow to recirculate and accordingly U decreases especially at the centre line.

The influences of the Reynolds number and Ar on the average Nusselt number on the bottom surface is graphically presented in Fig. 6. In all Ar, the average Nusselt number increases with increasing Reynolds number. This is because forced convection strengthens at higher Reynolds number and thus, heat transfer increases.

The results also show that the average Nusselt number increases as Ar reduces. When U_{max} at the centre of the microchannel decreases as Ar is decreased (it can be found from Fig. 5), flow velocity near the microchannel surface that is associated with the higher convective heat transfer coefficient is increased. Thus, by reduction in Ar, the heat transfer from the micrachannel walls to the nanofluid increases.

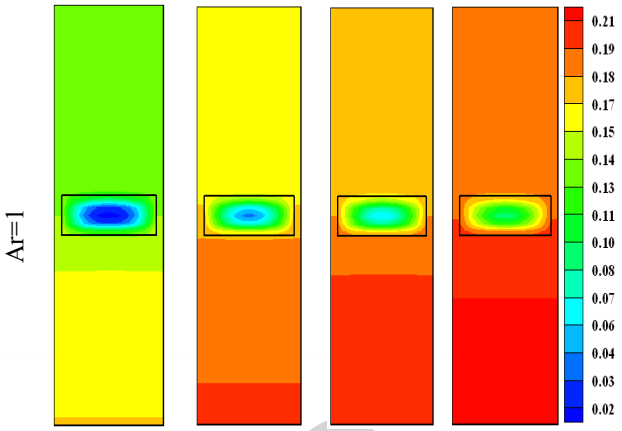

Fig. 4. Isotherms for with various Ar in the cross-section of the channel (Re=200).

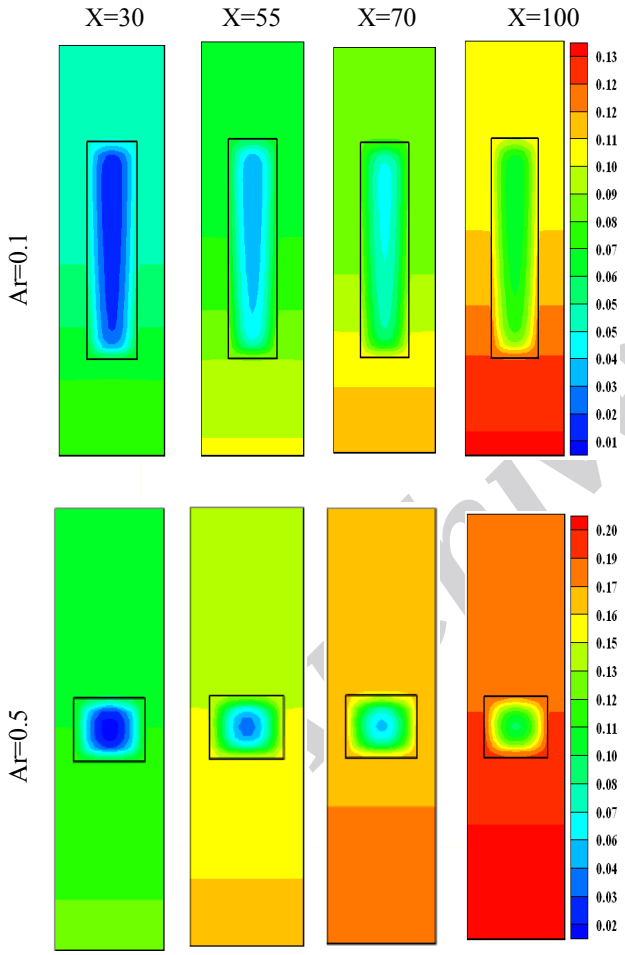

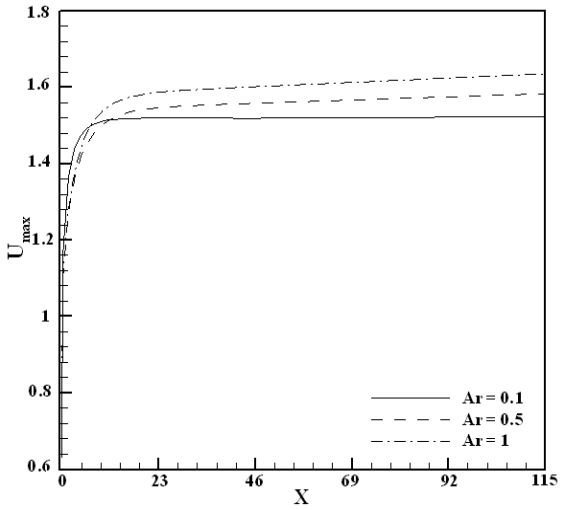

Fig. 5. Variation of maximum horizontal velocity along the channel centre line for various Ar (Re=200).

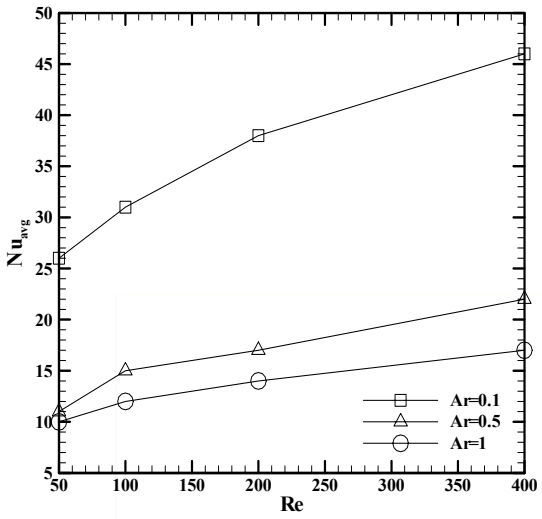

Fig. 6: Average Nusselt number on the bottom surface versus Reynolds number for various aspect ratios.

Fig. 7 shows values for thermal resistance at both the outlet and inlet channel for all considered Reynolds numbers and aspect ratios. The values of thermal resistance have an inverse correlation with heat transfer. Local convection coefficients are larger at the channel inlet than at the channel outlet because of entry effects. When more thermal energy is transferred to the nanofluid near the channel entrance, the surface temperature near the channel entrance will decrease and the resistance will be low. If less energy is transferred to the nanofluid near the channel entrance, the convection coefficient will be low, which will increase the surface temperature in this region as well as the resistance. As outlined in Fig. 7, rising Reynolds number causes to decrease in thermal resistance at both the channel outlet and inlet. For high Reynolds numbers, the surface temperatures became very close to the liquid inlet temperatures resulting in a low thermal resistance. Fig. 7 also confirms that the resistance will decrease as Ar reduces.

5. Conclusions

A numerical model was utilized to simulate a three dimensional fluid flow and heat transfer in a three-dimensional microchannel filled with Al_2O_3 - water nanofluid. Based on the present numerical study, the following results are obtained:

1- For all values of the Ar, the temperature in both nanofluid and microchannel wall increase versus increasing distance from the channel entrance.

2- The maximum dimensionless horizontal velocity along the centre line of the microchannel are affected by varying Ar. Velocity increases as the Ar increases.

3- Heat transfer from the micrachannel walls to the nanofluid (or average Nusselt number) increases as Ar decrease.

4- By decreasing Ar, the inlet and outlet thermal resistance decrease.

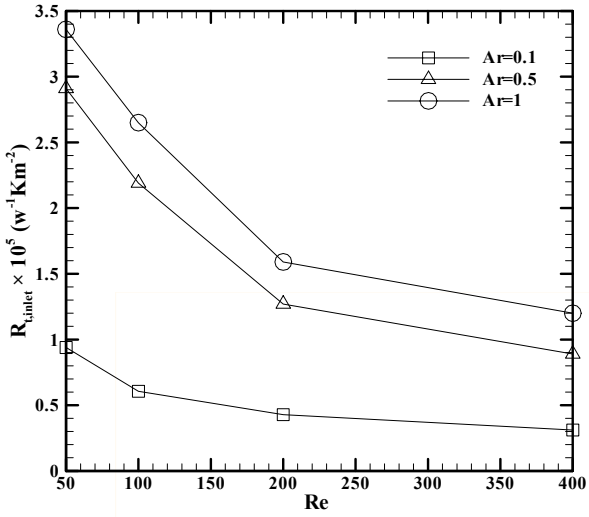

(a)

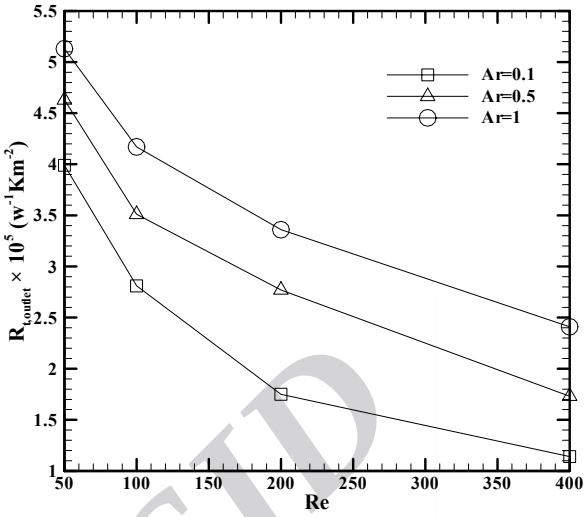

(b)

Fig. 7. Thermal resistance value versus Reynolds number for various aspect ratios.

References

[1] B.D. Tuckerman and R.F.W. Pease, IEEE Electr. Device Lett. EDL, 2 (1981), 136-147.

[2] J. Li, G.P. Peterson, IEEE Trans. Compon. Packag. Technol. 29 (1) (2006) 145–154

[3] K. Kawano, K. Minakami, H. Iwasaki, M. Ishizuka, Development of micro channels heat exchanging, in: R.A. Nelson Jr., L.W. Swanson, M.V.A. Bianchi, C. Camci (Eds.), HTD-Vol. 361-3/PID-Vol. 3, ASME, New York, (1998) 173–180.

[4] J.F. Tullius, R. Vajtai, Y. Bayazitoglu, Heat Transfer Engineering 32 (7–8) (2011) 527–541.

[5] S. Lee, S.U.S. Choi, PVP-vol. 342/MD-vol. 72, ASME, New York, (1996), 227–234.

[6] S.P. Jang, S.U.S. Choi, Appl. Thermal Eng, 26 (2006) 2457-2469.

[7] A. Raisi, B. Ghasemi and S.M. Aminossadati, Numerical Heat Transfer; Part A: Applications, 59 (2) (2011) 114-123.

[8] S.M. Aminossadati, A.Raisi and B.Ghasemi, Int. J. Non-Linear Mechanics, 46 (2011) 1373-1384.

[9] Justin D. Mlcak, N.K. Anand, Michael J. Rightley, Heat and Mass Transfer, 51 (2008) 5128-5137.

[10] G.A. Sheikhzadeh, M. Ebrahim Qomi, N. Hajialigol, A. Fattahi, Results in Physics, 2 (2012) 5-13

[11] D.C. Lo, D.L. Young, K. Murugesan, C.C. Tsai, M.H. Gou, Heat and Mass Transfer, 50 (2007) 479-484.